# Damping the floater motion of vertical-axis wind turbines using load optimisation

De Tavernier, D.; Viré, A.; Ferreira, C.

**DOI**
10.1088/1742-6596/1452/1/012042

**Publication date**
2020

**Document Version**
Final published version

**Published in**
Journal of Physics: Conference Series

# Damping the floater motion of vertical-axis wind turbines using load optimisation

# Damping the floater motion of vertical-axis wind turbines using load optimisation

**D. De Tavernier, A. Viré, C. Ferreira**

Delft University of Technology, Wind Energy, Kluyverweg 1, Delft, The Netherlands,

E-mail: d.a.m.detavernier@tudelft.nl

**Abstract.** In this work, we demonstrate to what extent it is possible to use load optimisation to aerodynamically damp the floater motion of vertical-axis wind turbines. The loadform of a VAWT can be altered to the desired objective using an individual blade-pitch schedule. A coupled hydro- and aerodynamic simulation tool is built solving the equation of motion of the floating system in which the hydrodynamic loads and (frequency-dependent) matrices are modelled using the potential flow theory and the aerodynamic loads are computed using the Actuator Cylinder model. A blade-pitch optimisation schedule is included to redistribute the loads over the actuator with the objective to counter-act the hydrodynamic loads as much as possible without significant power loss. Using the simulation tool, it is shown that an intelligently determined blade-pitch schedule can decrease the floater motion, however, the potential of reducing the floater motion is limited by the fact that the aerodynamic loads are significantly smaller than the hydrodynamic loads especially for rough sea states.

## 1. Introduction

Over the next 10 years, the wind energy industry anticipates that offshore installations will grow with 17% each year[1]. In this evolution, floating wind farms might open new perspectives. Deep-water areas with rich wind resources in waters beyond the reach of bottom-fixed technology become available. To make floating wind turbines economically viable, the use of conventional horizontal-axis wind turbines may not be the optimal design. Therefore, it is of interest to study the feasibility of other concepts such as vertical-axis wind turbines.[2] In particular the insensitivity to wind direction and the low center of gravity have caused a renewed surge of interest in VAWTs for floating, deep-offshore applications.[3]

### *1.1. Background*

A fundamental difference between bottom-fixed and floating turbines is the additional complexity introduced by the motion of the floating platform. Turbines are translating and rotating in 3 dimensions. Turbine motions due to wave excitations make the flow less predictable and may cause the turbine to operate outside of its design conditions. The turbine loads will vary more drastically compared to bottom-fixed turbines and as such increase fatigue issues. Therefore and amongst other reasons, it is of great interest to reduce the floater motion to its minimum.

For vertical-axis wind turbines (VAWTs) it has been shown feasible to redistribute the loads over the actuator using blade pitching to achieve various objectives. Houf[4] has shown numerically that blade-pitch can be used to minimise/maximise the thrust without losing power.

LeBlanc[5] experimentally showed that the thrust, and as such the wake, can be deflected using individual blade pitching.

It is believed that the principle of intelligently designing a blade-pitch schedule, and thus redistributing the loads over the actuator, could be used to counter-act the hydrodynamic loads, and as such aerodynamically damp the floater motion. For horizontal-axis wind turbines it has already been shown that blade-pitch can be used to damp fore-aft tower motion or additional structural vibrations[6]. In the S4VAWT project[7], it is demonstrated that controlling the blade pitch angle in survival conditions can result in lower responses.

### *1.2. Research objective*

In this paper, it will be studied whether the turbine loading can be used to aerodynamically damp the floater motion during normal operation. The blade-pitch schedule will be optimised such that the aerodynamic forces counter-act the hydrodynamic loads without significant power loss. The research question of this paper is formulated as: *'Can we reduce the floater motion of a vertical-axis wind turbine during normal operation by optimising the rotor loading using blade-pitch?'*. This work should serve as a proof-of-concept to identify the feasibility and the limits to aerodynamically damp the motion of the floating system.

## 2. Methodology

### *2.1. Turbine*

In this study a virtual floating 5MW vertical-axis wind turbine is considered. This floating system is inspired by the OC5 DeepCwind floating wind system design, in which a semi-submersible floating platform is carrying the NREL 5MW turbine[8]. The same floater is considered in this work, however, the HAWT is replaced by an equivalent VAWT with similar frontal area and power output inspired by Tescione[9].

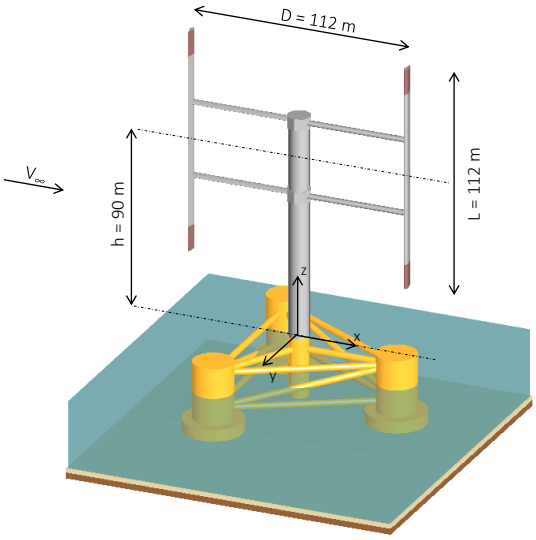


| DOF | Freq., f (Hz) | Period, P (s) |
|---|---|---|
| Surge | 0.00937 | 106.7 |
| Sway | 0.00890 | 112.3 |
| Heave | 0.0571 | 17.5 |
| Roll | 0.0305 | 32.8 |
| Pitch | 0.0308 | 32.5 |
| Yaw | 0.0124 | 80.8 |

Figure 1 & Table 1: An illustration of the floating turbine system and the experimentally obtained eigen-frequencies of the 6 degrees-of-freedom[8]

The turbine has a two-bladed rotor with a diameter of 112 m. The blade length is 112 m making the aspect ratio equal to 1. As for the NREL turbine, the turbine height is 90m. The rated wind speed of 11m/s. To match the power output of the HAWT, the rotor solidity is set to 0.1 and the tip speed ratio is 3. Except stated differently, all simulations are performed

at the rated wind speed and a rotational speed of 5.6rpm. The blades have a NACA0018 profile. In normal operational conditions, this reference rotor has a power coefficient of 0.5. A schematic representation is provided in Figure 1. The experimentally determined floater system frequencies, that may be of interest later in this work, are presented in the OC5 report[8] are given in Table 1.

*2.2. Aerodynamic and hydrodynamic modelling*

To model a floating vertical-axis wind turbine, a coupled simulation tool is built taking into account both the aerodynamics and hydrodynamics. The dynamics of a floating VAWT system consisting of a rotor, a floater and a mooring system, are represented by the equation of motion given by Equation 1. **M** is the mass matrix, **A** is the added mass matrix, **B** is the damping matrix, **C** is the hydrostatic stiffness matrix and **K** is the mooring stiffness. $x$, $\dot{x}$, $\ddot{x}$ are the displacement, velocity and acceleration of the platform, respectively. $F_{aero}$ and $F_{hydro}$ are the aerodynamic and hydrodynamic external forces. The $x$-vector is a 6-element vector prescribing the x-, y- and z-displacement and the x-, y- and z-rotation. The $F_{aero}$- and $F_{hydro}$-vector include the x-, y- and z-forces as well as the x-, y- and z-moments

$$(\mathbf{M} + \mathbf{A}) \cdot \ddot{x} + \mathbf{B} \cdot \dot{x} + (\mathbf{C} + \mathbf{K}) \cdot x = F_{aero} + F_{hydro} \tag{1}$$

**Hydrodynamic modelling:**

The hydrodynamic loads $F_{hydro}$ as well as the frequency dependent added mass matrix **A** and damping matrix **B** are computed using the program *WADAM*[10]. *WADAM* is a hydrodynamic tool used to analyse the interaction of (regular) waves with various frequencies with offshore structures. The body is discretised into panels and the hydrodynamic properties are calculated using a source-sink approach. Because of linearity, the problem can be decomposed into a diffraction and radiation problem. In the diffraction problem, the potential flow theory[11] is used to determine the wave excitation force when the body is at rest and interacting with incident waves. Potential flow implies that the flow is inviscid and irrotational. The velocity field $u$ can thus be described by the velocity potential $\Phi(x, t)$, as given in Equation 2. The pressure $p$ is computed using the unsteady Bernoulli equation.

$$u = \nabla\phi = \left(\frac{\partial\phi}{\partial x}, \frac{\partial\phi}{\partial y}, \frac{\partial\phi}{\partial z}\right) \tag{2}$$

By solving the radiation problem, in which the body is oscillating in its six degrees-of-freedom in absence of waves, the added mass, damping and restoring terms are determined. For severe sea states, the viscous forces and flow separation need to be taken into account. In this case, the potential flow-solution for large volume bodies is combined with Morison's viscous term. The results of the hydrodynamic matrices are obtained from Rivera-Arreba[12] in which the implementation of the model is verified using free decay tests and validated against CFD and experimental results.

**Aerodynamic modelling:**

The aerodynamic force vector $F_{aero}$ is computed using the Actuator Cylinder (AC) model. The Actuator Cylinder, developed by Madsen[13], is a 2D flow model extending the actuator disk concept. An actuation surface is introduced that coincides with the swept area of the rotor, which is a cylindrical surface for a VAWT. The reaction of the blade forces ($F_n$ and $F_t$) are applied on the flow as distributed body forces ($Q_n$ and $Q_t$) in the normal and tangential directions. The actuator cylinder concept is presented in Figure 2. The solution of the velocity

field around the actuator cylinder builds on the 2D, steady, incompressible Euler equations and the equation of continuity[14]. The induced velocities are prescribed by the volume forces and induced forces and consist of a linear and non-linear solution. The so-called *Mod-Lin* solution[15] uses only the linear version of the AC model and a correction to account for the non-linear part, instead of solving the computationally expensive non-linear solution. The non-linear part of the induced velocity is compensated using a correction factor $k_a$[16] and is calculated based on the relation between the induction factor $a$ and the thrust coefficient $C_T$. This relation includes that $C_T = 4a(1-a)$ for $a < 0.5$ as well as the Glauert correction for $a > 0.5$. This *Mod-Lin* solution method requires less resources and still delivers accurate results[17].

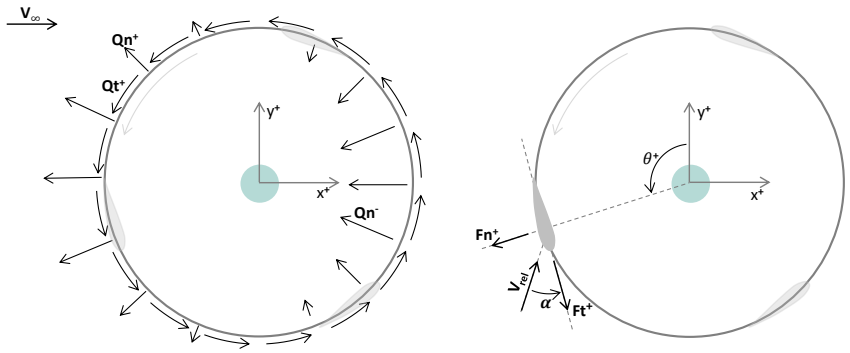


Figure 2: Representation of the 2D actuator cylinder with sign convention.

With the velocity field known, the blade element theory is applied to determine the 2D aerodynamic forces on the rotor. The 2D results are then integrated along the rotor height to obtain the 3D loads. Because this work only deals with a proof-of-concept of aerodynamically damping the floater motion, no dynamic inflow model or dynamic stall model are included for simplicity.

### *2.3. Blade-pitch optimisation*

Individual blade-pitch will be used to alter the overall force vector to fulfil the desired objective and as such damp the floater motion. The objective in this research is set to counter-act the hydrodynamic forces as much as possible, and as such to either maximize the x-force, minimize the x-force or maximise the y-force without losing power, depending on the instantaneous needs. Additional constraints are defined to the maximum blade-pitch deflection and the blade-pitch rate. For every timestep, the required blade-pitch schedule and as such the corresponding turbine loading are determined. An optimisation scheme is set up using the build-in Matlab function *fmincon* in which the design variables are the blade-pitch angle at discrete azimuthal positions.

## 3. Results

### *3.1. Blade-pitch optimisation*

An intelligently designed blade-pitch schedule can be used to obtain several objectives. In most research, blade pitching is used to operate at optimal loading and maximise the power output. In the present case, the ultimate goal will be to alter the overall load vector to counter-act the hydrodynamic forces. Therefore, different objectives become of interest such as (1) minimise the x-force with a constraint on power loss, (2) maximise the x-force with a constraint on power loss and (3) maximise the y-force with a constraint on power. These objectives might be obtained by redistributing the loads over the 2D actuator. The incoming wind speed is in the positive x-direction.

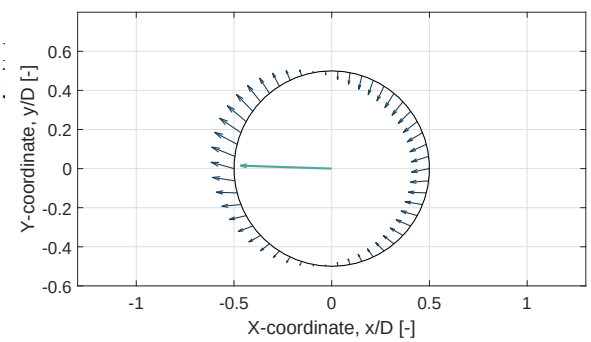


*(a) Reference - Forcefield*

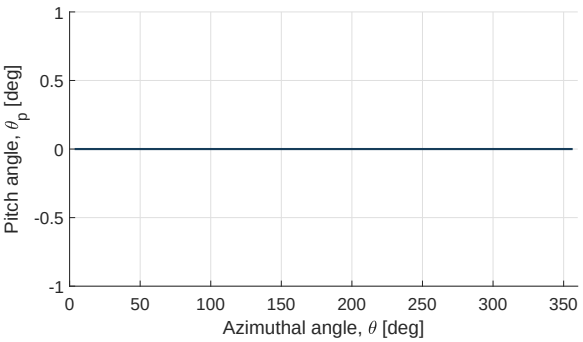


*(b) Reference - Pitch schedule*

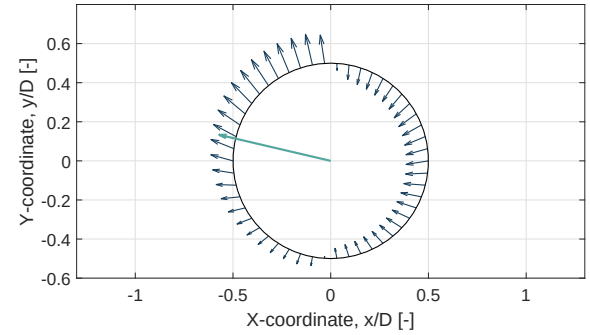


*(c) Max $C_P$ - Forcefield*

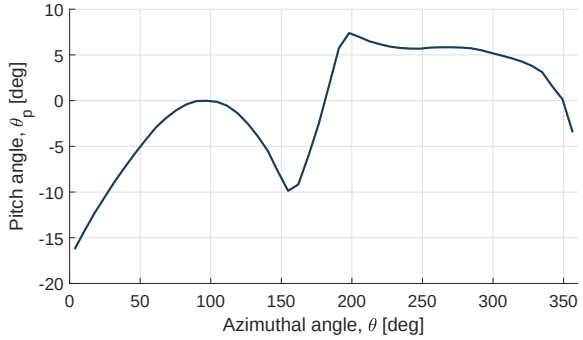


*(d) Max $C_P$ - Pitch schedule*

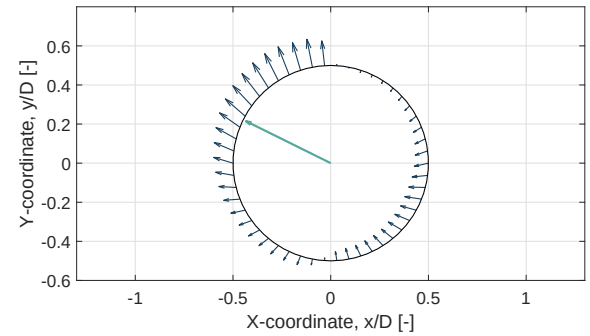


*(e) Min $C_x$ - Forcefield*

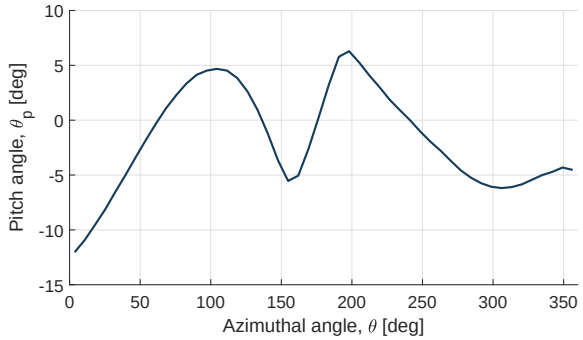


*(f) Min $C_x$ - Pitch schedule*

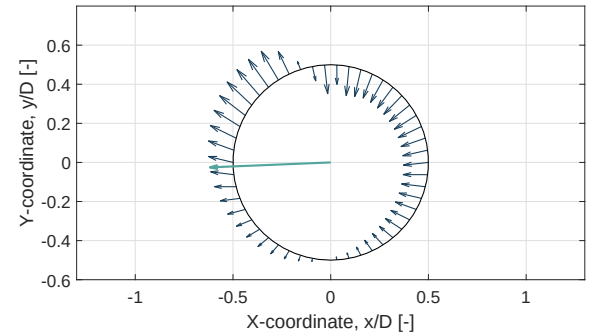


*(g) Max $C_x$ - Forcefield*

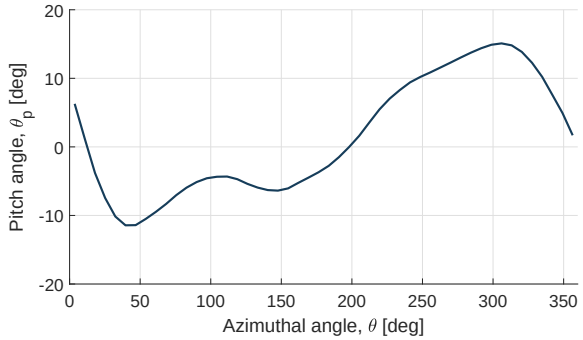


*(h) Max $C_x$ - Pitch schedule*

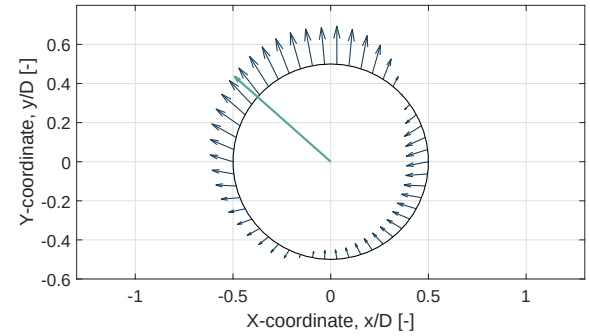


*(i) Max $C_y$ - Forcefield*

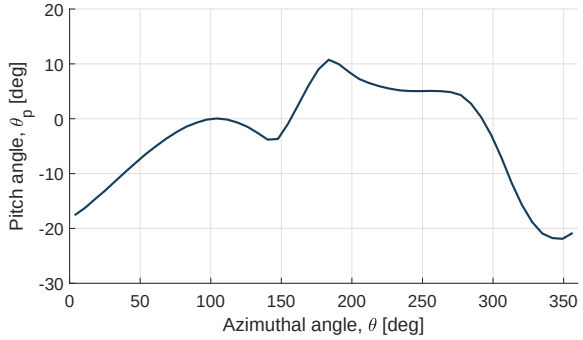


*(j) Max $C_y$ - Pitch schedule*

Figure 3: Optimised loading and pitch schedule for different objectives: (a) & (b) as a reference without objective, (c) & (d) for maximum power, (e) & (f) for minimum thrust without power loss, (g) & (h) for maximum thrust and no power loss and (i) & (j) for maximum side force and no power loss.

The results for these objectives for the reference turbine at rest are presented in Table 2 and Figure 3. In Table 2, the power coefficient, x-force coefficient and y-force coefficient in optimised conditions for the various objectives are provided. In Figure 3, the corresponding force fields and pitch schedules are presented. The results of the turbine with zero pitch are presented as a reference.

From the results, one may observe that an intelligently selected blade-pitch schedule might allow (for this particular turbine) to increase the power coefficient with around 11%. If the objective is to minimise the thrust, a reduction of almost 5% can be achieved while constraining the power loss. With the same constraint, the thrust can be increased by 38%. A pitch schedule also allows to generate a side force. This capability might be valuable and could be used to damp the floater motion of a vertical-axis wind turbine.

Table 2: Optimised power and force coefficients for different objectives

| Objective | Power coefficient, $C_P$ [-] | X-force coefficient, $C_x$[−] | Y-force coefficient, $C_y$ [-] |
|---|---|---|---|
| Reference | 0.49260 | 0.67979 | 0.02334 |
| Max $C_P$ | 0.55315 | 0.86092 | 0.20103 |
| Min $C_x$ | 0.49242 | 0.65413 | 0.31562 |
| Max $C_x$ | 0.49319 | 0.93224 | -0.03804 |
| Max $C_y$ | 0.49273 | 0.74091 | 0.65746 |

*3.2. Floater motion*

Using the simulation code coupling the hydrodynamics and aerodynamics, the turbine movement in time and space can be determined. The 6 degrees-of-freedom location of the turbine is prescribed by the equations of motion given in Equation 1 in which the state vector includes the surge, sway and heave location and the pitch, roll and yaw angle.

The hydrodynamic loads, associated with excitations from incoming waves on the platform aligned with the incoming wind, mainly depend on the sea state considered. Regular waves from mild to extreme, adopted from the OC4 project description[18], are considered in this work. For sea state values lower than 2, the sea is considered calm. Starting from a sea state of 5, sea conditions could be considered rough. In Table 3 a summary is provided of the sea state definitions considered in this work.

Table 3: Sea state definitions with regular waves: sea state 1 is calm, sea state 8 is an extremely rough sea state.

| Sea state | Wave period, $T$ [s] | Wave height, $H$ [m] |
|---|---|---|
| 1 | 2.0 | 0.09 |
| 2 | 4.8 | 0.67 |
| 3 | 6.5 | 1.40 |
| 4 | 8.1 | 2.44 |
| 5 | 9.7 | 3.66 |
| 6 | 11.3 | 5.49 |
| 7 | 13.6 | 9.14 |
| 8 | 17.0 | 15.24 |

In Figure 4, the 6 degrees-of-freedom floater motion of the reference turbine in three sea states is provided. Until timestep 0s, the external loads are only composed of the hydrodynamic loads. From timestep 0s, the turbine is activated and the aerodynamic loads are added to the equation of motion. The presence of the turbine aerodynamic thrust causes a step in the surge

motion and pitch motion, and a small step in the sway and roll motion. The aerodynamic torque is causing a jump in the yaw angle. The heave motion is mainly caused by the hydrodynamic forces, and thus the presence of the aerodynamic forces does not cause a significant effect.

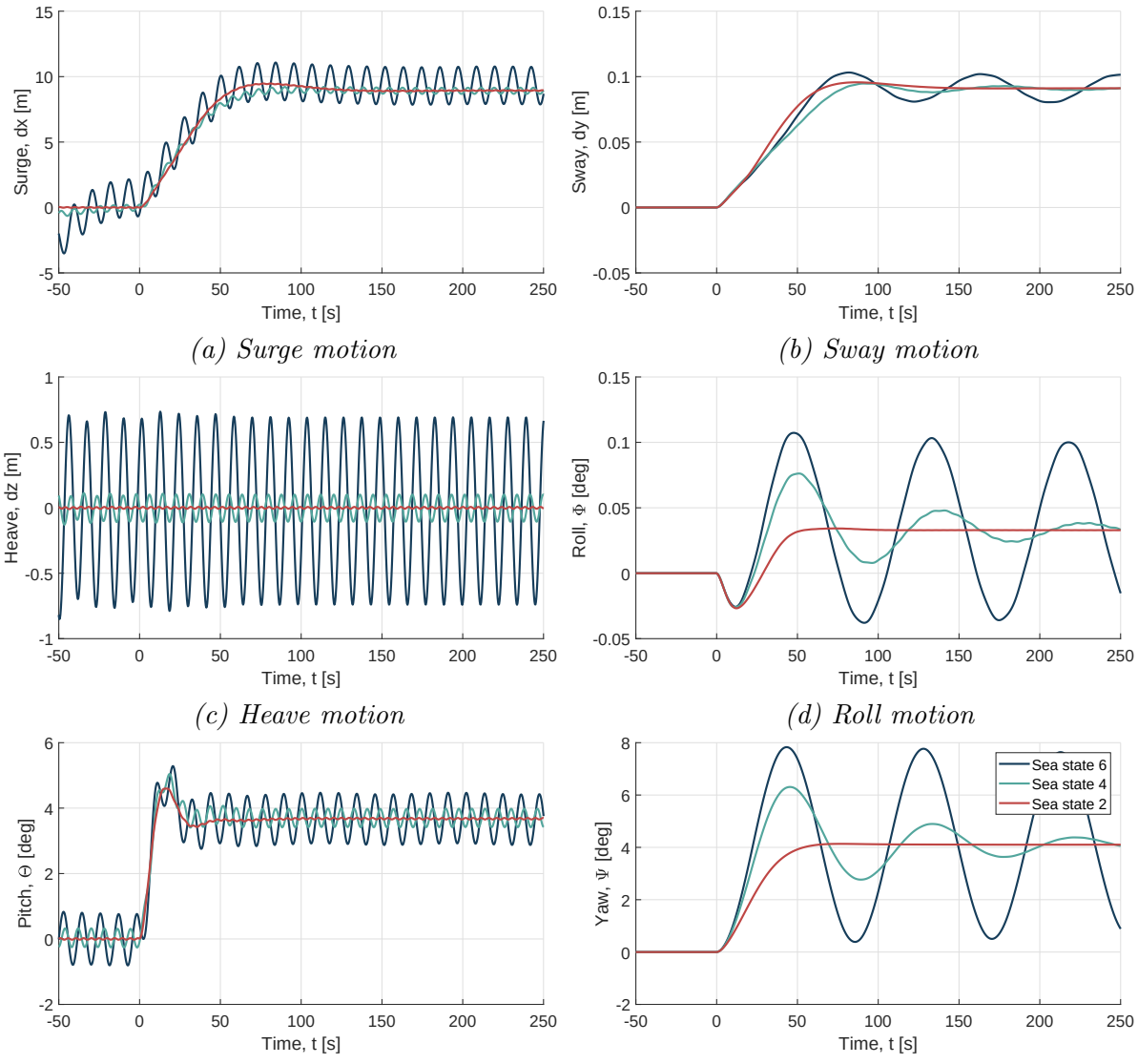


*(a) Surge motion* *(b) Sway motion*

*(c) Heave motion* *(d) Roll motion*

*(e) Pitch motion* *(f) Yaw motion*

Figure 4: 6-degree floater motion of the reference turbine in time for three different sea states at rated wind conditions: (1) sea state 6: T = 11.3s, H = 9.14m, (2) sea state 4: T = 8.1s, H = 2.44m, (3) sea state 2: T = 4.8s, H = 0.67m. The turbine is activated at t=0s.

The high frequency oscillations dominating the surge, heave and pitch motions, are caused by the wave frequency. The secondary lower frequency that is dominating the sway, roll and yaw motion is corresponding to the eigen-frequency of the yaw motion. By activating the turbine, the yaw eigen-frequency is excited and lowly damped. The cyclic yaw motion with a period around 80s, causes the aerodynamic forces to oscillate at that frequency. This is resulting in the fact that the secondary frequency originally caused by the yaw motion is appearing on nearly all other degrees-of-freedom but clearly visible in the sway motion and roll rotation. Depending on the mode and wave state, some motions are highly damped and others only slightly damped.

Comparing the different sea states, one can observe that all sea states are showing similar behaviours where, as expected, sea state 6 is predicting larger platform motions than sea state 2.

For the same three sea states, the hydrodynamic and aerodynamic external forces are provided in Figure 5 for the last 100 seconds of the same time series. The hydrodynamic forces increase for increasing sea state and oscillate at the wave frequency. The aerodynamic forces are mainly dominated by the relative velocity of the rotor, composed by the incoming wind speed and the velocity caused by the motion of the rotor. The component caused by the turbine motion depends on the motion amplitude and frequency. Due to this, the amplitude of the aerodynamic force is not necessarily expected to increase with increasing sea state. Again a secondary oscillation (on top of the wave frequency) with a period of 80s (close to the eigen-frequency of the yawing motion) is visible.

Besides this, note that the hydrodynamic forces are in general one or more orders of magnitude larger than the aerodynamic forces. This will serve as a limiting factor in the attempt to prove the concept of damping the floater motion using the aerodynamic forces.

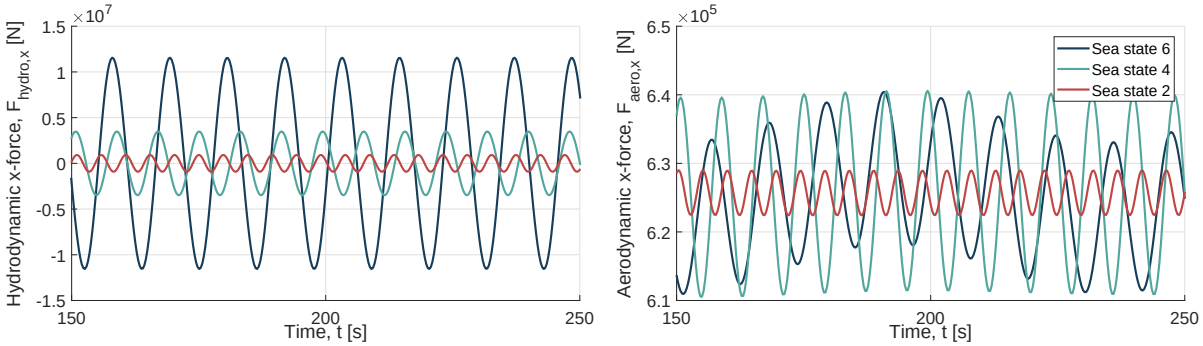


*(a) Hydrodynamic forces* *(b) Aerodynamic forces*

Figure 5: External force (hydrodynamic and aerodynamic) applied to the floating reference turbine in three different sea states at rated wind conditions: (1) sea state 6: T = 11.3s, H = 9.14m, (2) sea state 4: T = 8.1s, H = 2.44m, (3) sea state 2: T = 4.8s, H = 0.67m.

### *3.3. Damping floater motion*

When activating the blade-pitch optimisation routine in the aerodynamic modelling of the floating reference turbine, the floater motion can be studied again. In this paper, the objective for the blade-pitch optimisation is set to damp the x-motion as much as possible considering a constraint in power loss and thus to counteract the x-force. In this paper, the focus is set to the x-motion (surging) since this is the most pronounced motion.

In Figure 6 the results are provided of the reference turbine where no power loss is allowed. These figures provide the external x-force and surging motion for three different sea states. A distinction is made between the case without active blade-pitch schedule and the case with active blade-pitch schedule.

One can see that for sea state 2 individual blade-pitch clearly decreases the external x-force. This consequently causes the amplitude of the surging motion to reduce. For sea state 4, the effect of using variable blade-pitch is less pronounced in the external x-force. This is due to the fact that the hydrodynamic forces are one order of magnitude larger than the aerodynamic forces, limiting the capabilities of the aerodynamic forces. Although the effect of the external x-force is small, it is still capable to slightly decrease the amplitude of the surging motion. At sea state 6, when removing the low frequency component with a high-pass filter, it can be concluded that the surging amplitude is nearly the same with and without blade-pitch.

To demonstrate the effect of the optimised blade-pitch schedule on the turbine performance, Figure 7 is provided. This figure presents the corresponding thrust coefficient for the three sea state conditions with and without blade-pitch. The thrust coefficients are normalised purely with respect to the incoming wind and thus do not include the extra velocity component created by the motion.

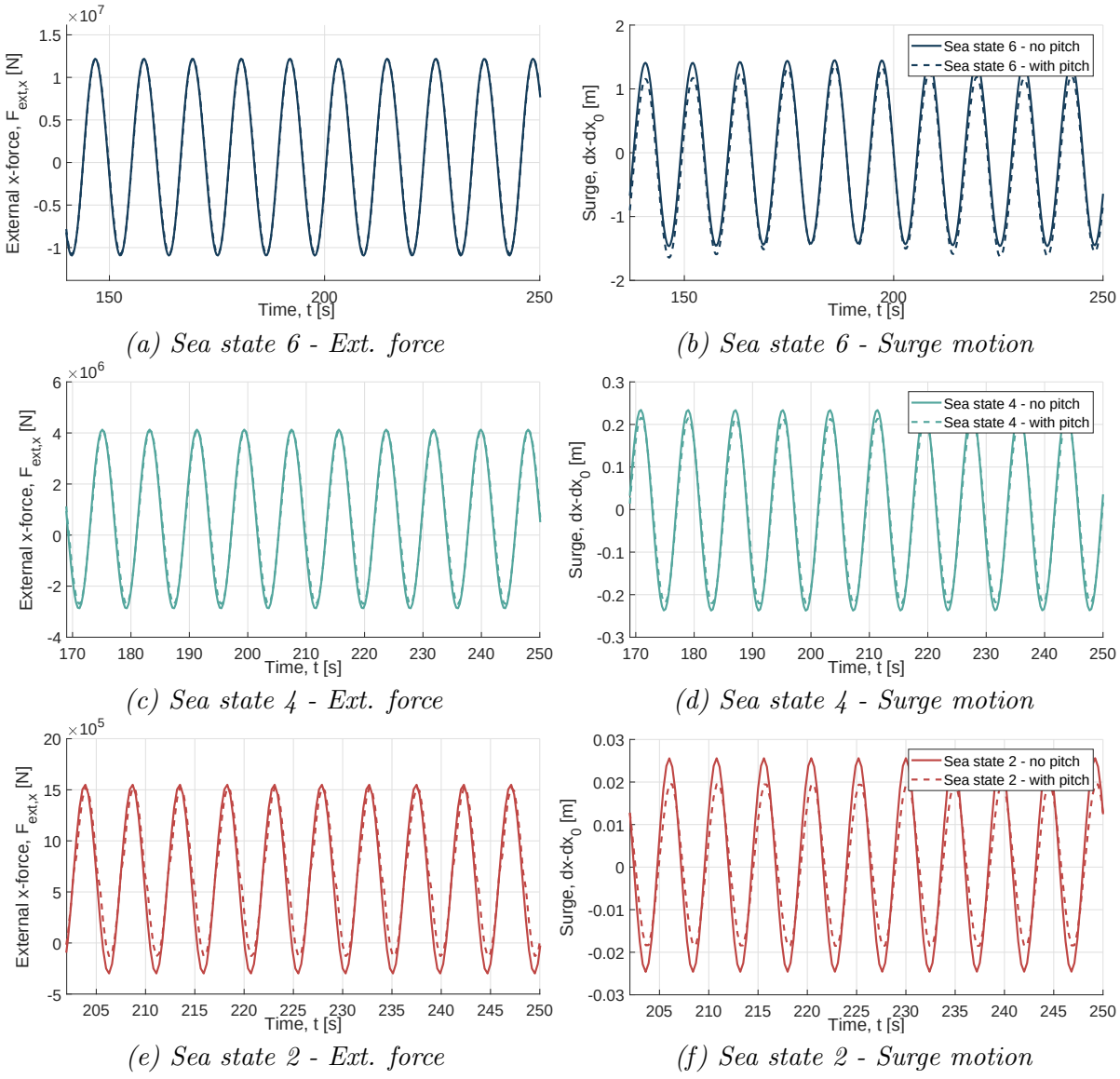


*(a) Sea state 6 - Ext. force* *(b) Sea state 6 - Surge motion*

*(c) Sea state 4 - Ext. force* *(d) Sea state 4 - Surge motion*

*(e) Sea state 2 - Ext. force* *(f) Sea state 2 - Surge motion*

Figure 6: External force and surge motion in time of the reference turbine in three different sea states at rated wind conditions: (1) sea state 6: T = 11.3s, H = 9.14m, (2) sea state 4: T = 8.1s, H = 2.44m, (3) sea state 2: T = 4.8s, H = 0.67m.

The thrust coefficient, basically being the objective of the pitch optimisation, is significantly different in case of blade pitching. It is minimised and rather constant in case of a positive hydrodynamic force, and it is maximised when the hydrodynamic force is negative. In this case it is counteracting the hydrodynamic forces to its maximum. In absence of a blade-pitch schedule the variation of the thrust coefficient is significantly different for the different sea state. Including an optimised blade-pitch schedule, the minimum and maximum thrust coefficients are

rather similar for all sea states. The power coefficient is basically serving as a constraint to the pitch optimisation. In this example, it is said that the power cannot be lower than in case there is no blade-pitch schedule in the same floating conditions.

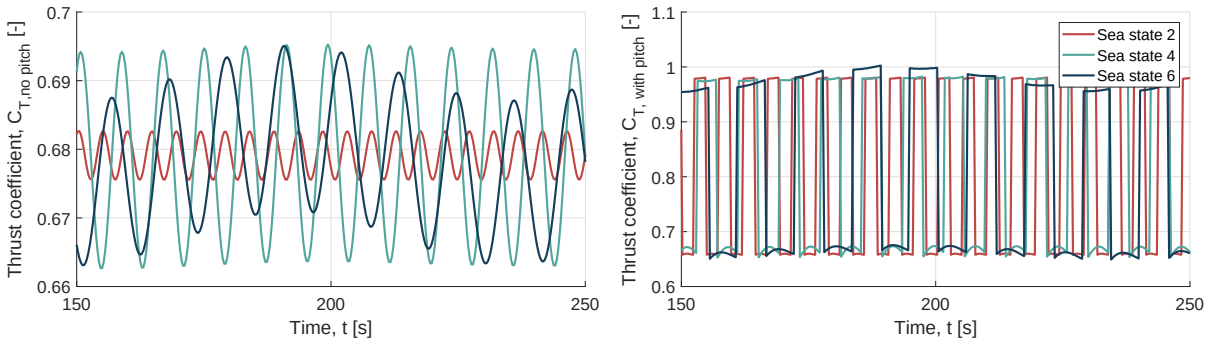


*(a) $C_T$ - no blade-pitch* *(b) $C_T$ - with blade-pitch*

Figure 7: Thrust coefficient in time of the reference turbine in three different sea states at rated wind conditions: (1) sea state 6: T = 11.3s, H = 9.14m, (2) sea state 4: T = 8.1s, H = 2.44m, (3) sea state 2: T = 4.8s, H = 0.67m.

So far, all simulations are run with an incoming velocity of 11 m/s, which is the rated wind speed and with a constraint stating that no power loss is allowed. The simulations are also repeated for two other wind speeds: at 5 m/s which is below the rated velocity and 17 m/s which is above the rated velocity. A summary of the results is provided in Figure 8(a). This graph proves that the surging motion can be damped up to 25% depending on the sea state for an incoming wind speed of 11 m/s. The larger the waves, and thus the hydrodynamic forces, the smaller the potential of using load optimisation. At a higher incoming wind speed, the forces generated by the rotor are larger and as such the potential to damp the floating motion increases. At 17 m/s, up to 55% of the motion can be damped. The opposite is true for the lowest incoming wind speed. Note that in reality, an incoming wind speed of 17m/s will hardly occur in combination of sea state 2 since there is a clear correlation between the sea state and wind speed.

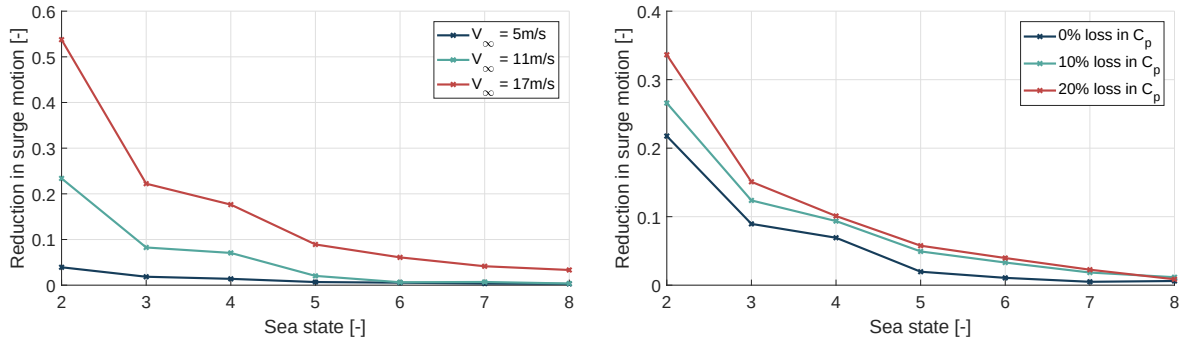


*(a) Various incoming wind speeds* *(b) Various constraints on power*

Figure 8: Reduction of surging amplitude using pitch for various sea states and (a) various incoming wind speeds or (b) various constraints on the power.

When relaxing the constraint on the power, e.g. by allowing a power loss of 10% or 20%, the surging motion can be damped further. This is proven by Figure 8(b). This graph shows that

with a power loss of 20% the reduction of the surging motion can be increased with up to 10% at low sea states. For rough sea states, the potential decreases again.

These results support the proof-of-concept of using force vector optimisation to damp the floater motion of vertical-axis wind turbines. However, it has been clear that the potential to reduce the surging motion is clearly limited by the fact that the aerodynamic force is significantly smaller than the hydrodynamic force, especially for rough sea states. At small sea states, the reduction in surging motion can be reduced up to 50%, however, this should be put in perspective since the surging motion at this sea state is even in absence of load optimisation already smaller than 1m. At this stage, only the surge motion was considered. Because no attention is put to the other degrees-of-freedom, this might cause that for some of the other degrees-of-freedom a small increase in the motion could be identified. However, a similar approach could be introduced to damp the motion in the other degrees-of-freedom.

## 4. Conclusion

In this paper, a numerical study is performed to demonstrate to what extent the floater motion of a vertical-axis wind turbine in normal operation can be reduced by optimising the rotor loading. Individual blade-pitch is used to redistribute the loads and as such alter the overall load vector in the desired direction to counteract the hydrodynamic forces. Additionally a constraint is introduced on the loss of power.

A coupled hydro- and aerodynamics model is built. The dynamics of the floating VAWT are represented by the equations of motion of a rigid body under aero- and hydrodynamic loading. The hydrodynamic loads and frequency dependent matrices are determined using the potential flow hydrodynamic tool *WADAM*. The aerodynamic forces are computed using the Actuator Cylinder model.

A demonstration is given to show that an intelligently designed blade-pitch schedule can be used to obtain several objectives amongst them: (1) maximise the power output, (2) minimise the x-force constraining the power loss, (3) maximise the x-force constraining the power loss and (4) maximise the y-force constraining the power loss. Connecting this blade-pitch optimisation scheme with the coupled model, showed that the rotor loading (using blade-pitch) can be selected in such a way it can reduce the surging motion of the floating system. It has been observed that in general using load optimisation the surging motion can be damped at calm sea states but it has only negligible effect in rough sea states. At rated wind speed, a reduction up to 35% has been identified depending on the constraint added to the power loss. For looser power constraint, a larger reduction is observed. Also, it is found that the observed reduction in the surging motion, increases with the incoming wind speeds.

The results presented in this paper support the proof-of-concept of optimising the loading using blade-pitch to damp the floater motion of vertical-axis wind turbines. However, it is identified that the potential to reduce the (surging) motion is limited by the fact that the aerodynamic loads are significantly smaller than the hydrodynamic loads especially for rough sea states. This work only studied the physical feasibility, however, so far it is not yet considered in further detail how this can be practically implemented. Also, the main attention is set to the surging motion and in case the wind and waves are aligned. The same kind of analysis could be repeated considering the damping of the other degrees-of-freedom.

## References

[1] A. Cronin, ETIP Wind, The way forward for offshore wind possible scenarios, Presentation, EERA DeepWind, 2019.
[2] S. Watson, A. Moro, V. Reis et al., Future emerging technologies in the wind power sector: A European perspective, Renewable and sustainable energy reviews, 113(109270), 2019.
[3] U.S. Paulsen, M. Borg, H.A. Madsen, et al. Outcomes of the DeepWind Conceptual Design. Energy Procedia; 80(329-341), 2015.

[4] D.P. Houf, Active pitch control of a vertical axis wind turbine, Msc thesis, Technical University of Denmark and Delft University of Technology, 2016.
[5] B.P. LeBlanc, C. Ferreira, Experimental determination of thrust loading of a 2-bladed vertical axis wind turbine, Journal of Physics: Conf. series, 1037(022043), 2018.
[6] L.Y. Pao, K.E. Johnson, Control of wind turbines: approaches, challenges, and recent developments, IEEE Control systems magazine, 31(2), pp. 44-62, 2011.
[7] F. Huij, E. Vlasveld, M. Gormand, F. Savenije, M. Caboni, B. LeBlanc, C. Ferreira, K. Lindenburg, S. Gueydon, W. Otto, B. Paillard, Integrated design of a semi-submersible floating vertical axis wind turbine (VAWT) with active blade pitch control, Journal of Physics: Conf. Series, 1104(012022), 2018.
[8] A. Robertson, J. Jonkman, F. Wendt, A. Goupee, H. Dagher, Definition of the OC5 DeepCwind semisubmersible floating system, Technical report, 2016.
[9] G. Tescione, On the aerodynamics of a vertical axis wind turbine wake: an experimental and numerical study, PhD thesis, Delft University of Technology, 2016.
[10] C.H. Lee, Wamit – Theory manual, Massachusetts Institute of Technology, 1995.
[11] J. Hess, A. Smith, Calculation of non-lifting potential flow about arbitrary three-dimensional bodies, Journal of Ship Research, 8(1), pp. 22–44, 1964.
[12] I. Rivera-Arreba, N. Bruinsma, E.E. Bachynski, A. Viré, B.T. Paulsen, N.G. Jacobsen, Modeling of a semisubmersible floating offshore wind platform in severe waves, Journal of offshore mechanics and Arctic engineering, 141(061905-1), 2019.
[13] H.A. Madsen, On the ideal and real energy conversion in a straight bladed vertical axis wind turbine, PhD thesis, Aalborg University, 1983.
[14] J. Katz, A. Plotkin, Low speed aerodynamics, United States of America, Cambridge University Press, second ed., 2001.
[15] H.A. Madsen, T. Larsen, L. Vita, U.S. Paulsen, Implementation of the Actuator Cylinder flow model in the HAWC2 code for aeroelastic simulations on Vertical Axis Wind Turbines, 51st AIAA Aerospace Sciences Meeting including the New Horizons Forum and Aerospace Exposition, 2013.
[16] Z. Cheng, H.A. Madsen, Z. Gao, T. Moan, Aerodynamic modeling of floating vertical axis wind turbines using the actuator cylinder flow method, Energy Procedia, 94, pp. 531-543, 2016.
[17] H.A. Madsen, U.S. Paulsen, L. Vita, Analysis of VAWT aerodynamics and design using the Actuator Cylinder flow model, Journal of Physics: Conf. Series, 555(012065), 2014.
[18] A. Robertson, J. Jonkman, M. Masciola, H. Song, A. Goupee A. Coulling and C. Luan, Definition of the Semisubmersible Floating System for Phase II of OC4, Technical Report NREL, 2014.